

Two magnetization plateaus in the kagome fluoride $\text{Cs}_2\text{LiTi}_3\text{F}_{12}$

Ryu Shirakami,¹ Hiroaki Ueda,¹ Harald O. Jeschke,² Hiroki Nakano,³ Shintaro Kobayashi,⁴ Akira Matsuo,⁵ Tôru Sakai,^{3,6} Naoyuki Katayama,⁴ Hiroshi Sawa,⁴ Koichi Kindo,⁵ Chishiro Michioka,¹ and Kazuyoshi Yoshimura¹

¹*Department of Chemistry, Graduate School of Science, Kyoto University, Kyoto 606-8502, Japan*

²*Research Institute for Interdisciplinary Science, Okayama University, Okayama 700-8530, Japan*

³*Graduate School of Material Science, University of Hyogo, Kamigori, Hyogo 678-1297, Japan*

⁴*Department of Applied Physics, Graduate School of Engineering, Nagoya University, Nagoya 464-8603, Japan*

⁵*Institute for Solid State Physics, The University of Tokyo, Kashiwanoha, Kashiwa, Chiba 277-8581, Japan*

⁶*National Institutes for Quantum and Radiological Science and Technology (QST), SPring-8, Sayo, Hyogo 679-5148, Japan*



(Received 25 August 2019; published 1 November 2019)

We synthesized a kagome fluoride $\text{Cs}_2\text{LiTi}_3\text{F}_{12}$ with $S = 1/2$ spins, and studied magnetic properties of the compound. The temperature dependence of the magnetic susceptibility indicates that it has dominant antiferromagnetic interactions and that it has no magnetic order down to 2 K. We found two magnetization plateaus in its magnetization process approximately at $1/3$ and $0.8 \mu_B$ per Ti. The monoclinic crystal structure gives four inequivalent nearest-neighbor exchange interactions. Our density functional theory calculations suggest that three of them are antiferromagnetic and one of them is weakly ferromagnetic, resulting in a magnetic system composed of antiferromagnetically coupled linear chains and Δ chains. This explains the observed suppression of magnetic order. Numerical diagonalization gives a magnetization curve in good agreement with the experimental results.

DOI: [10.1103/PhysRevB.100.174401](https://doi.org/10.1103/PhysRevB.100.174401)

I. INTRODUCTION

Quantum Heisenberg spin systems on a kagome lattice have attracted much attention from both theoretical and experimental viewpoints. In the last decade and a half, a number of kagome antiferromagnets with $S = 1/2$ have been extensively studied [1]. Much of this research is driven by the desire to realize highly frustrated Hamiltonians where strong quantum effects lead to an exotic state of matter, the quantum spin liquid [2]. Most $S = 1/2$ kagome antiferromagnets are Cu^{2+} based materials, which include Cu containing minerals, such as herbertsmithite [3], vesignieite [4,5], kapellasite [6], centennialite [7], and Cu based fluorides $\text{Cs}_2T\text{Cu}_3\text{F}_{12}$ ($T = \text{Ti}, \text{Zr}, \text{Hf}, \text{Sn}$) [8]. However, the Cu^{2+} ion has relatively large spin-orbit coupling, and thus a large Dzyaloshinsky-Moriya interaction [9]. In the context of the search for spin liquids, this is undesirable as it may induce magnetic ordering.

Recently, we found a new series of kagome fluorides $A_2BM_3F_{12}$ ($A, B = \text{alkali metal ion}, M = \text{Ti}, \text{V}, \text{and Cr}$) [10–12]. Among them, the Ti compounds have spin $S = 1/2$. Compared to the $S = 1/2$ magnetic ion Cu^{2+} , Ti^{3+} has much smaller spin-orbit coupling. We have already reported the crystal structure and magnetic properties of the three Ti^{3+} kagome compounds $\text{Rb}_2\text{NaTi}_3\text{F}_{12}$, $\text{Cs}_2\text{NaTi}_3\text{F}_{12}$, and $\text{Cs}_2\text{KTi}_3\text{F}_{12}$ [10]. Owing to lattice distortion from rhombohedral to monoclinic, they have a slightly distorted kagome lattice. We revealed that the magnetic states of kagome antiferromagnets strongly depend on lattice distortion. Indeed, our theoretical study clarified that the lattice distortions makes the kagome lattice magnetically anisotropic [13].

In this paper we report the crystal structure and magnetic properties of the new kagome magnet $\text{Cs}_2\text{LiTi}_3\text{F}_{12}$ which is

a member of the above-mentioned $A_2B\text{Ti}_3\text{F}_{12}$ family. This compound has a slightly distorted kagome lattice of Ti^{3+} . Since the crystal structure of $\text{Cs}_2\text{LiTi}_3\text{F}_{12}$ is qualitatively the same as other $A_2B\text{Ti}_3\text{F}_{12}$, we can use the new material to systematically study the effect of lattice distortion on the magnetism of $S = 1/2$ kagome antiferromagnets. The measured magnetic properties of $\text{Cs}_2\text{LiTi}_3\text{F}_{12}$ are similar to those of $\text{Cs}_2\text{KTi}_3\text{F}_{12}$; therefore, it comes as a surprise that the magnetic models are different between these two. Moreover, $\text{Cs}_2\text{LiTi}_3\text{F}_{12}$ has smaller antiferromagnetic interactions than the previously studied $A_2B\text{Ti}_3\text{F}_{12}$, allowing us to study high field magnetism. In high fields, $\text{Cs}_2\text{LiTi}_3\text{F}_{12}$ shows not only the $1/3$ magnetic plateau but also a magnetic plateau with a larger magnetization. We discuss details of the magnetic properties of $\text{Cs}_2\text{LiTi}_3\text{F}_{12}$.

II. METHODS

Polycrystalline samples of $\text{Cs}_2\text{LiTi}_3\text{F}_{12}$ were synthesized with a solution method under N_2 atmosphere. Single crystals of $\text{Cs}_2\text{LiTi}_3\text{F}_{12}$ were grown with a flux method using alkali metal chlorides in a Ni crucible under Ar atmosphere. A polycrystalline sample of a nonmagnetic isostructural compound $\text{Cs}_2\text{KGa}_3\text{F}_{12}$ was prepared with a solid state reaction in a Cu tube under Ar atmosphere.

Powder x-ray diffraction measurements were performed at room temperature using Miniflex600 (Rigaku) with a $\text{Cu } K\alpha$ source. X-ray diffraction data of a single crystal with a typical size of $90 \times 80 \times 30 \mu\text{m}^3$ were obtained using a Rigaku R-AXIS RAPID-S diffractometer with $\text{Mo } K\alpha$ radiation. The sample was cooled down to approximately 150 K using a nitrogen-gas-flow-type refrigerator. The structural parameters

including anisotropic displacement parameters were refined using a full matrix least-squares method with the SHELXL-97 software [14].

Polycrystalline samples were used for magnetic susceptibility and magnetization measurements, and one single crystal was used for heat capacity measurements. DC magnetization was measured in a temperature range of 2–300 K using a superconducting quantum interference device magnetometer (Quantum Design MPMS-XL) in the Research Center for Low Temperature and Materials Sciences, Kyoto University. Magnetization processes up to 75 T were measured using an induction method with a multilayer pulsed magnet at the International MegaGauss Science Laboratory of the Institute for Solid State Physics, the University of Tokyo. Heat capacity measurements were performed using a commercial relaxation calorimeter (Quantum Design PPMS-14LHS).

To understand our experimental observations, we carried out a two-step calculation. The first step is the determination of the electronic structure and magnetic interaction parameters of $\text{Cs}_2\text{LiTi}_3\text{F}_{12}$ using density functional theory (DFT) calculations with the all electron full potential local orbital (FPLO) [15] basis and the generalized gradient approximation (GGA) [16] exchange correlation functional. We account for strong electronic correlations on the Ti^{3+} ions using the GGA+ U [17] correction. The Hund's rule coupling for Ti 3d was fixed at $J_H = 0.64$ eV [18]. We used an energy mapping technique to determine the most important exchange interactions in $\text{Cs}_2\text{LiTi}_3\text{F}_{12}$ [19–21]. By lowering the symmetry of $\text{Cs}_2\text{LiTi}_3\text{F}_{12}$ to $P1$, all six Ti^{3+} ions in one unit cell become inequivalent, and 15 collinear spin configurations with different total energies can be created. We fit these energies against the Heisenberg Hamiltonian written as $\mathcal{H} = \sum_{i<j} J_{ij} \mathbf{S}_i \cdot \mathbf{S}_j$ without double counting of bonds. This calculation allows us to resolve all “nearest-neighbor” exchange couplings in the kagome plane.

The second step of our calculation is numerical diagonalization of finite-size clusters with Heisenberg interactions determined from the DFT calculations. Our numerical diagonalizations are carried out based on the Lanczos and/or Householder algorithms in the subspace characterized by $\sum_j S_j^z = M_z$, where the z axis is taken as the quantized axis of each $\mathbf{S} = 1/2$ spin operator \mathbf{S}_j at site j . Our numerical diagonalizations provide us with the lowest energy of the Heisenberg Hamiltonian with the number of sites N in the subspace belonging to M_z . The energy is denoted by $E(N, M_z)$. To obtain the steplike magnetization process when the Zeeman term $-2\mu_B H \sum_j S_j^z$ is added to \mathcal{H} , we use the relation $2\mu_B H = E(N, M_z + 1) - E(N, M_z)$ which determines the magnetic field H for the occurrence of the magnetization increase from M_z to $M_z + 1$. Note here that the isotropy of the system is assumed and that the saturation magnetization is given by NS . Therefore, the normalized magnetization per magnetic site is given by $M = M_z/(NS)$, which corresponds to the magnetization per Ti site in units of μ_B . Some of the Lanczos diagonalizations were carried out using an MPI-parallelized code that was originally developed in the study of Haldane gaps [22]. The usefulness of our program was confirmed in various large-scale parallelized calculations [23–35]. We carried out our diagonalizations of the systems with $N = 24, 30$, and 36 . The

TABLE I. Atomic coordinates and isotropic displacement parameters of $\text{Cs}_2\text{LiTi}_3\text{F}_{12}$ at 150 K. The space group is $P2_1/m$, and the structural parameters are $a = 12.877(6)$ Å, $b = 7.594(5)$ Å, $c = 7.162(6)$ Å, $\beta = 125.30(4)^\circ$, and $Z = 2$. The residual indices are $R = 0.0392$ and $\omega R = 0.1025$. The numbers in parentheses are standard deviations in the last significant figures.

Atom	x	y	z	U (Å ²)
Cs1	0.61894(4)	0.75	0.61986(6)	0.02070(14)
Cs2	0.13016(3)	0.25	0.62174(6)	0.01798(14)
Li1	0.7311(11)	0.25	0.5117(19)	0.026(2)
Ti1	0	0	0	0.0113(2)
Ti2	0.5	0	0	0.0101(2)
Ti3	0.76963(9)	0.25	0.05607(18)	0.0106(2)
F1	0.0222(5)	0.25	0.9397(8)	0.0310(10)
F2	0.5909(2)	0.4344(3)	0.3107(4)	0.0170(5)
F3	0.0981(2)	0.9336(3)	0.8669(4)	0.0164(5)
F4	0.1525(3)	0.0164(4)	0.2946(5)	0.0291(6)
F5	0.5631(3)	0.75	0.1001(6)	0.0170(7)
F6	0.3477(2)	0.5467(3)	0.0046(4)	0.0173(5)
F7	0.1755(3)	0.75	0.6323(6)	0.0187(7)
F8	0.3002(4)	0.75	0.2573(6)	0.0194(7)

shapes of the finite-size clusters are taken to be the same ones as were used in the previous study [13].

III. RESULTS AND DISCUSSION

By using a solution method, we succeeded in synthesizing polycrystalline samples of $\text{Cs}_2\text{LiTi}_3\text{F}_{12}$. Powder x-ray diffraction measurements revealed that $\text{Cs}_2\text{LiTi}_3\text{F}_{12}$ has a monoclinic structure. In addition, we obtained brown crystals of $\text{Cs}_2\text{LiTi}_3\text{F}_{12}$ with a typical size of $2 \times 2 \times 2$ mm³. However, we found that large crystals are composed of several domains, which is likely due to monoclinic deformation with decreasing temperature. Single crystal x-ray diffraction measurement revealed details of the crystal structure, as summarized in Table I. No disorder of the constituent ions is observed. This structure is qualitatively the same as that previously reported for $A_2B\text{Ti}_3\text{F}_{12}$ compounds [10], and it can be regarded as an ordered structure of the cubic modified pyrochlore AM_2F_6 [36]. Ordering of Li^+ and Ti^{3+} in the pyrochlore lattice of M results in formation of a kagome lattice of Ti^{3+} . Thus, this structure consists of kagome layers which are made up of corner-sharing TiF_6 octahedra, separated by nonmagnetic Cs^+ ions and Li^+ ions. Moreover, TiF_6 octahedra are compressed along axes which point out of the kagome plane, and this distortion leads to a small lifting of the degeneracy between the three t_{2g} orbitals. Therefore, the single 3d electron of Ti^{3+} occupies the $3d_{xy}$ orbitals which are almost parallel to the kagome plane.

Reflecting the monoclinic distortion, $\text{Cs}_2\text{LiTi}_3\text{F}_{12}$ has three crystallographically different Ti sites. Both Ti1 and Ti2 form one-dimensional (1D) chains along the b axis and the chains are bridged by Ti3. Therefore, there are four inequivalent exchange interactions. The Ti-Ti distances and the Ti-F-Ti bond angles are within the range of 3.734–3.797 Å and 134.2° – 142.7° , respectively. These ranges are slightly larger than those of other $A_2B\text{Ti}_3\text{F}_{12}$ compounds. The large distances between two Ti ions of approximately 3.7 Å indicate that

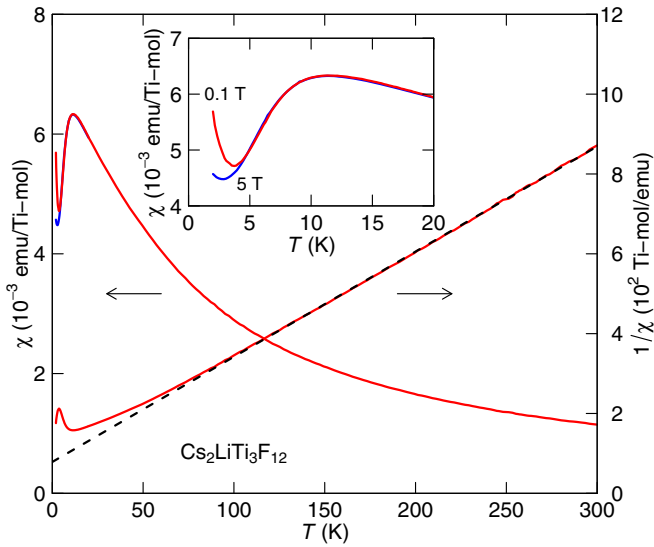


FIG. 1. Temperature dependence of the magnetic susceptibility χ and of the inverse of the magnetic susceptibility χ^{-1} (right scale). The black dashed line indicates the result of the Curie-Weiss fit. The inset shows the magnetic field dependence at low temperatures.

direct exchange interactions between two Ti are negligibly small. Thus, the dominant interactions are superexchange interactions. The obtained Ti-F-Ti bond angles are much larger than 90° which leads to the expectation that the magnetic exchanges between nearest neighbor Ti ions are antiferromagnetic.

The temperature dependence of the magnetic susceptibility χ and of the inverse susceptibility are shown in Fig. 1. No magnetic ordering is observed down to 2 K. At high temperatures, the χ^{-1} - T curve is almost linear and is well fitted using the Curie-Weiss law $\chi = C/(T - \theta_{CW})$, where C is the Curie constant and θ_{CW} is the Curie-Weiss temperature. The fitting gives $C = 0.380$ emu K/Ti mol, and $\theta_{CW} = -29.8$ K. The Curie constant gives an effective Bohr magneton number $p_{\text{eff}} = 1.74$, which is in good agreement with the theoretical value of 1.73 for $S = 1/2$ and $g = 2$. The negative value of the Curie-Weiss temperature indicates that the dominant magnetic interactions are antiferromagnetic, as expected from Ti-F-Ti bond angles. According to mean-field theory, the Curie-Weiss temperature is given by $\theta_{CW} = -nJS(S + 1)/3k_B$, where n is the number of nearest neighbor spins, J is the nearest neighbor interaction, and k_B is Boltzmann constant. Using $n = 4$ for kagome lattice, we obtained an average nearest neighbor exchange coupling $J = 29.8$ K. The value of J for $\text{Cs}_2\text{LiTi}_3\text{F}_{12}$ is the smallest among four $A_2\text{BTi}_3\text{F}_{12}$ compounds. Those of $\text{Rb}_2\text{NaTi}_3\text{F}_{12}$, $\text{Cs}_2\text{NaTi}_3\text{F}_{12}$, and $\text{Cs}_2\text{KTi}_3\text{F}_{12}$ are 43, 44, and 47 K, respectively [10].

In the low temperature region, χ - T shows a broad maximum approximately at $12 \text{ K} \simeq J/3$, which implies short range order effects [37]. This behavior is expected in low dimensional (both one- and two-dimensional) systems where magnetic order is absent. In our previous study, χ - T curves of $A_2\text{BTi}_3\text{F}_{12}$ strongly depend on the distortion of the kagome lattice. Among them, a broad maximum at $T \simeq J/3$ was observed also in χ of $\text{Cs}_2\text{KTi}_3\text{F}_{12}$, which has the smallest distortion and arguably the most frustrated Hamiltonian of

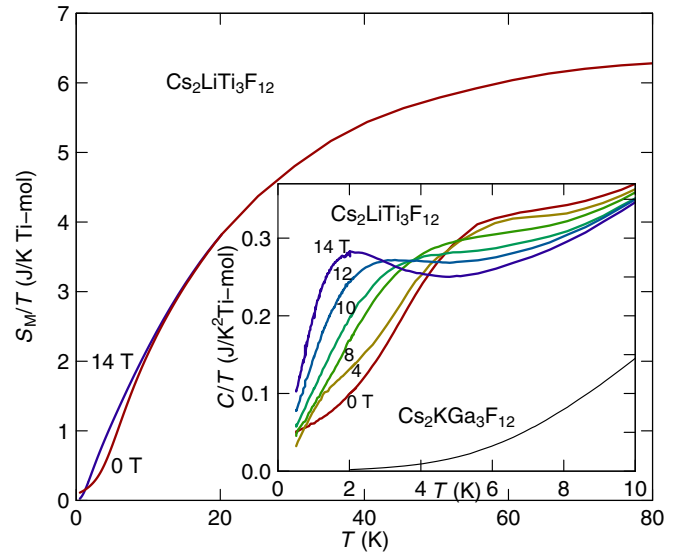


FIG. 2. Magnetic entropy of $\text{Cs}_2\text{LiTi}_3\text{F}_{12}$ up to 80 K. The inset shows the heat capacity divided by temperature under various magnetic fields. The data for nonmagnetic $\text{Cs}_2\text{KGa}_3\text{F}_{12}$ are also plotted to show the lattice contribution.

the three compounds [10,13]. A theoretical study proposed that the susceptibility of the $S = 1/2$ kagome antiferromagnet exhibits a broad maximum at $T \sim J/6$ [38]. The difference between the theory and experiment is considered to arise from the distortion of the kagome lattice, which is similar to $\text{Rb}_2\text{SnCu}_3\text{F}_{12}$ [39]. The small upturn of the susceptibility measured under 0.1 T below 4 K is due to magnetic impurities, because it is suppressed under 5 T. The amount of magnetic impurity that causes an upturn at low temperatures is evaluated to be approximately 1% from the Curie constant obtained by fitting the χ - T curve in this region.

To investigate the details of the magnetic states of $S = 1/2$ $\text{Cs}_2\text{LiTi}_3\text{F}_{12}$, we measured the temperature dependence of the heat capacity C under several magnetic fields using a relatively large crystal grown with the flux method. We applied the magnetic field along the [111] direction of the crystal in the cubic indices. The heat capacity divided by temperature C/T is plotted in the inset of Fig. 2. Under zero field, the absence of λ -like anomalies indicates no long range magnetic ordering down to 0.5 K. The C/T - T curves show the magnetic field H dependence below 12 K. The temperature of 12 K corresponds to the temperature where the χ - T curve shows a broad maximum indicating short range magnetic ordering. Moreover, each C/T curve shows a broad peak at T_{max} , and T_{max} decreases with increasing H . This behavior is likely due to formation of short range magnetic order which is restrained by the magnetic field. This behavior is very similar to that of $\text{Cs}_2\text{KTi}_3\text{F}_{12}$.

By subtracting the lattice contribution and integrating C/T , we evaluated the magnetic entropy S_M . The calculated S_M gradually increases with increasing temperature, and reaches 5 J/K approximately at $-\theta_{CW}$, and then saturates above 80 K. The magnetic entropy at 80 K is slightly larger than the theoretical value $R \ln 2 = 5.76 \text{ J/K}$ for $S = 1/2$. This discrepancy is likely due to errors of specific heat and lattice contribution.

TABLE II. Nearest-neighbor intersite Ti-Ti distances and labels for exchange couplings in $\text{Cs}_2\text{LiTi}_3\text{F}_{12}$. Two couplings J_{3a} and J_{3b} correspond to the same distance but connect two symmetry inequivalent Ti sites. Note that J_5 and J_{10} correspond to interlayer couplings.

d (Å)	Ti1		Ti2		Ti3	
Ti1	3.7970	J_{3b} J_B	6.2814	J_5	3.7339	J_1 J_D
Ti2	6.2814	J_5	3.7970	J_{3a} J_A	3.7695	J_2 J_C
Ti3	3.7339	J_1 J_D	3.7695	J_2 J_C	6.8155	J_{10}

Using the experimentally obtained crystal structure and θ_{CW} , we determined the exchange couplings. As mentioned before, the distorted kagome lattice has three Ti sites; the 1D Ti1 chain and Ti2 chain are bridged by Ti3. And hence, it has four “nearest-neighbor” exchange couplings. Here we use two kinds of labels for the exchange couplings, which are summarized in Table II. One kind of labels J_n are couplings labeled according to the physical structure, ordered by increasing Ti-Ti distance as shown in Table II. As there are two identical distances Ti1-Ti1 and Ti2-Ti2 along the 1D chains, which however are symmetry inequivalent and do not have the same exchange, they are called J_{3a} , J_{3b} . The other kind of labels J_A to J_D are related to the model for the distorted kagome lattice; J_A and J_B are couplings along the one-dimensional chains, and J_C and J_D are those in the zigzag chains bridging J_A and J_B chains, respectively. Note that J_A is always assigned to be the largest 1D chain coupling. The exchanges are visualized in Fig. 3. We can determine the relevant value of the interaction strength U by demanding that the Curie-Weiss temperature calculated as $\theta_{\text{CW}} = -\frac{2}{3}S(S+1)[\frac{2}{3}J_1 + \frac{2}{3}J_2 + \frac{1}{3}J_{3a} + \frac{1}{3}J_{3b} + \frac{2}{3}J_5 + \frac{1}{3}J_{10}]$ match the experimentally determined value. The Heisenberg Hamiltonian parameters of $\text{Cs}_2\text{LiTi}_3\text{F}_{12}$ obtained by energy mapping are shown in Fig. 3 and in Table III for seven values of the interaction strength U . The value $U = 2.4$ eV required to match the experimental value of θ_{CW} is reasonable for Ti^{3+} and agrees well with the values that describe the magnetic exchange of the sister compounds $\text{RbNaTi}_3\text{F}_{12}$, $\text{CsNaTi}_3\text{F}_{12}$, and $\text{CsKTi}_3\text{F}_{12}$ [13]. The selected interlayer couplings J_5 and J_{10} are very small and will be neglected in the further discussion. The obtained parameters are shown in Table IV.

Interestingly, the model we obtain for $\text{Cs}_2\text{LiTi}_3\text{F}_{12}$ is quite different from those for the other known compounds. It is characterized by strong antiferromagnetic spin chains J_A . This

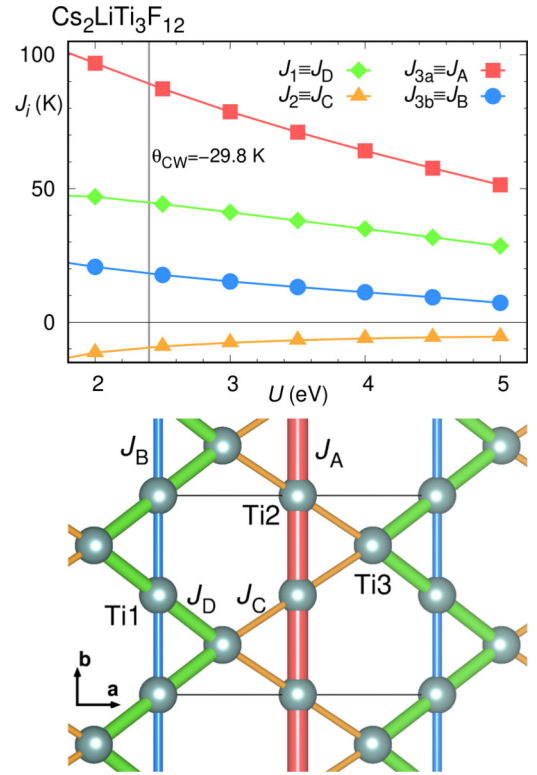


FIG. 3. Exchange couplings of $\text{Cs}_2\text{LiTi}_3\text{F}_{12}$ determined by energy mapping. (Top) Seven sets of couplings determined from GGA+ U calculations at different interaction strengths U . The gray line marks the interactions, found by interpolation, that match the experimental Curie-Weiss temperature $\theta_{\text{CW}} = -29.8$ K. (Bottom) Visualization of the exchange strength in the Ti^{3+} kagome lattice—the bond cross-sectional areas are proportional to the size of the couplings. 1D Ti1 chains and Ti2 chains are formed through J_B and J_A , respectively. These chains are bridged by Ti3 atoms through J_D and J_C , respectively.

is coupled to the kagome lattice environment by *ferromagnetic* couplings J_C with a strength $|J_C/J_A| = 0.104$. Two thirds of the Ti^{3+} ions in the plane form anisotropic Δ chains, with a ratio $J_D/J_B = 2.46$. Our previous study clarified exchange couplings for other $A_2\text{BTi}_3\text{F}_{12}$ fluorides [13]; $\text{Rb}_2\text{NaTi}_3\text{F}_{12}$ has very small J_D and it consists of antiferromagnetic spin chains with J_B and anisotropic Δ chains with $J_C/J_A = 0.292$; $\text{Cs}_2\text{NaTi}_3\text{F}_{12}$ has relatively small J_C and it is considered

TABLE III. Exchange couplings of $\text{Cs}_2\text{LiTi}_3\text{F}_{12}$ calculated within GGA+ U at $J_H = 0.64$ eV and $8 \times 8 \times 8$ k points. The line in bold is obtained by requiring that the set of couplings yield the experimental Curie-Weiss temperature $\theta_{\text{CW}} = -29.8$ K.

U (eV)	$J_1 = J_D$ (K)	$J_2 = J_C$ (K)	$J_{3a} = J_A$ (K)	$J_{3b} = J_B$ (K)	J_5 (K)	J_{10} (K)	θ_{CW} (K)
2.0	46.9(1)	-11.3(1)	96.8(2)	20.7(2)	-0.1(1)	0.9(2)	-31.6
2.4	44.8(1)	-9.3(1)	89.1(2)	18.2(2)	-0.1(1)	0.7(1)	-29.8
2.5	44.2(1)	-9.0(1)	87.3(1)	17.7(1)	-0.1(1)	0.6(1)	-29.3
3.0	41.1(1)	-7.6(1)	78.7(1)	15.3(1)	-0.0(1)	0.4(1)	-26.9
3.5	38.0(1)	-6.7(1)	71.1(1)	13.2(1)	-0.0(1)	0.2(1)	-24.5
4.0	34.9(1)	-6.0(1)	64.1(1)	11.2(1)	0.0(1)	0.1(1)	-22.2
4.5	31.7(1)	-5.6(1)	57.6(1)	9.3(1)	0.0(1)	0.1(1)	-19.9
5.0	28.5(1)	-5.4(1)	51.4(1)	7.3(1)	0.1(1)	0.0(2)	-17.5

TABLE IV. Exchange couplings for $\text{Cs}_2\text{LiTi}_3\text{F}_{12}$ determined by energy mapping, using the GGA+ U exchange correlation functional with U values that reproduce the experimental Curie-Weiss temperatures $\theta_{\text{CW}} = -29.8$ K. See Fig. 3 for the assignment of J_A , J_B , J_C , and J_D .

Material	J_A (K)	J_B/J_A	J_C/J_A	J_D/J_A
$\text{Cs}_2\text{LiTi}_3\text{F}_{12}$	89.1	0.204	-0.104	0.503

to consist of antiferromagnetic spin chains with J_A and nearly isotropic Δ chains with $J_D/J_B = 0.967$; $\text{Cs}_2\text{KTi}_3\text{F}_{12}$ has almost the same J_B , J_C , J_D . Although the temperature dependence of χ for $\text{Cs}_2\text{LiTi}_3\text{F}_{12}$ is very similar to that of $\text{Cs}_2\text{KTi}_3\text{F}_{12}$, the models are completely different.

Based on the model Hamiltonian, we can develop an approximate expectation for the magnetization process. As the overall strength of J_D and J_B couplings is 0.503 and 0.204 of J_A , respectively, the saturation of the Δ chain is expected to be reached while the J_A spin chain shows a slow linear increase of magnetization [40]. At these low fields, the Δ chain will exhibit a $1/2$ magnetization plateau [41] which results in a $1/3$ magnetization plateau of the full system as it affects only two thirds of the Ti^{3+} ions. The $1/3$ magnetization plateau should be offset by a small, slightly increasing contribution from the J_A antiferromagnetic spin chain. Due to the large anisotropy, the Δ chain should show a jump to full saturation [41].

Now, let us investigate the behavior of the magnetization process of $\text{Cs}_2\text{LiTi}_3\text{F}_{12}$ through both experiment and calculation, results of which are shown in Fig. 4. We experimentally measured the magnetization process up to 75 T at 1.3 and 4.2 K. First, let us observe the characteristic behavior of our experiment based on the lower-temperature measurement. By increasing H from 0 T, M starts to increase with a finite slope. Around $H \sim 7$ T, there appears an inflection point of $M \sim 0.04 \mu_B$ per Ti. The inflection point will be discussed in comparison with our numerical-diagonalization result. At about 15 T, M increases with a considerable gradient. This corresponds to the fact that the broad peak in C/T moves to almost 0 K at 14 T. At around $H \sim 36$ T, another inflection point appears at $M \sim 0.37 \mu_B$. There is a possibility that the inflection point is related to the $1/3$ magnetization plateau behavior that was mentioned in the discussion of the Δ chain in the previous paragraph. By further applying H , M increases again at 50 T until approximately 70 T. Above 70 T, M exhibits a behavior of smaller gradients, which suggests a plateau behavior. The magnetic moment at this magnetization plateau is approximately $0.8 \mu_B$.

To analyze the behavior of the experimental M , we carried out numerical-diagonalization calculations, results of which are shown by steplike magnetization processes in Fig. 4. In the following, the comparison between the experimental result and the numerical result will be discussed. The experimental inflection point of $M \sim 0.37 \mu_B$ is close to $M = (1/3) \mu_B$ but seems slightly larger than $M = (1/3) \mu_B$; in theoretical results, on the other hand, the plateau just at $M = (1/3) \mu_B$ is unclear because the results of $N = 30$ and 36 show only small widths at $M = (1/3) \mu_B$ although the result of $N = 24$ shows a large width at $M = (1/3) \mu_B$. Instead, magnetizations $M = (4/9) \mu_B$ for $N = 36$ and $M = (2/5) \mu_B$ for $N = 30$

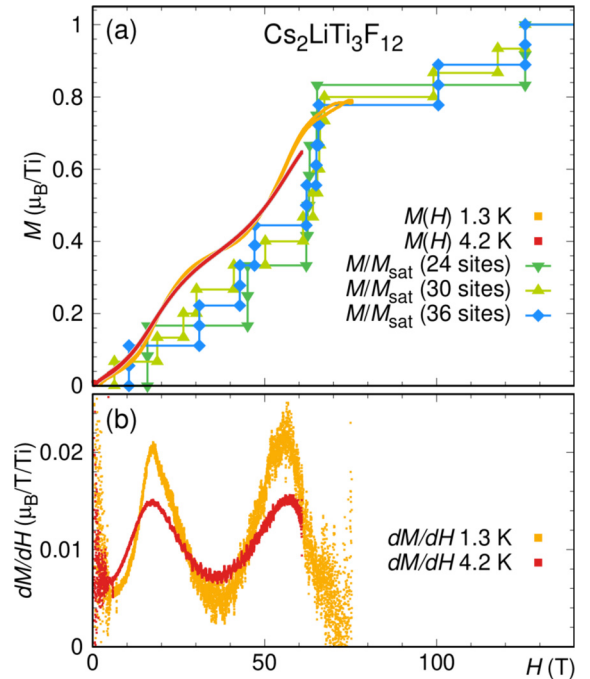


FIG. 4. (a) Magnetization curves of $\text{Cs}_2\text{LiTi}_3\text{F}_{12}$ measured at 4.2 and 1.3 K up to 75 T and theoretical spontaneous magnetization normalized by the saturation magnetization for system sizes $N = 24$, $N = 30$, and $N = 36$, and (b) differential curves of magnetization as a function of magnetic field. Abrupt increases of magnetization are observed at approximately 18 and 50 T. The magnetization curves show $1/3$ and 0.8 magnetization plateau at about 37 and 70 T, respectively.

show large widths. These theoretical behaviors are possibly related to the experimental $M \sim 0.37 \mu_B$ that is larger than $M = (1/3) \mu_B$. However, the field $H \sim 36$ T of this inflection point is smaller than the field range of $M = (4/9) \mu_B$ for $N = 36$ and $M = (2/5) \mu_B$ for $N = 30$. The reason is unclear at present. The present experimental measurement certainly detects the lower-field inflection point of $M \sim 0.04 \mu_B$ at $H \sim 7$ T. A similar inflection point was also observed in the case of $\text{Cs}_2\text{KTi}_3\text{F}_{12}$ [10]. Our result for $N = 36$ reveals a large width of $M = (1/9) \mu_B$ for $N = 36$. There is a possibility that our theoretical large width is related to the experimental inflection point. For further investigation of whether or not the experimental inflection point suggests the plateau behavior, theoretical studies by numerical diagonalizations for larger clusters giving higher resolution results will be required.

The most marked point is the behavior around $M \sim 0.8 \mu_B$. Our theoretical results reveal a plateau behavior approximately between 60 and 125 T. On the other hand, the low-temperature experimental result clearly reveals small gradients of M above 70 T. The small gradients suggest that our experimental measurement matches the behavior of the low-field side edge of the plateau in the theoretical results. In the magnetization process of the Δ chain, we expect a significant jump of the magnetization just before saturation [41]. This would correspond to the maximum of dM/dH at 55 T in $\text{Cs}_2\text{LiTi}_3\text{F}_{12}$. Since $2/3$ of Ti atoms form the Δ chain, saturation of the Δ chain gives $(2/3) \mu_B$. We think

that saturation of the Δ chain plus a small magnetization of the 1D chain could lead to a $0.8 \mu_B$ magnetization plateau in $\text{Cs}_2\text{LiTi}_3\text{F}_{12}$.

Note also that a behavior of a plateau with a large M near the saturation was not observed in $\text{Cs}_2\text{KTi}_3\text{F}_{12}$ owing to the limitation of the magnetic field in Ref. [10], although the existence of a plateau with the same height for $\text{Cs}_2\text{KTi}_3\text{F}_{12}$ was theoretically predicted [13]. Reference [13] also suggested the existence of a plateau with a large M near the saturation for $\text{Cs}_2\text{NaTi}_3\text{F}_{12}$ and $\text{Rb}_2\text{NaTi}_3\text{F}_{12}$. The present agreement of the plateau at around $M \sim 0.8 \mu_B$ for $\text{Cs}_2\text{LiTi}_3\text{F}_{12}$ between the experiment and theory suggests that higher-field measurements for $\text{Cs}_2\text{KTi}_3\text{F}_{12}$, $\text{Cs}_2\text{NaTi}_3\text{F}_{12}$, and $\text{Rb}_2\text{NaTi}_3\text{F}_{12}$ will be interesting future studies. The above explanation of $0.8 \mu_B$ magnetization plateau for $\text{Cs}_2\text{LiTi}_3\text{F}_{12}$ is different from those for the other Ti kagome fluorides, which all have differently distorted kagome lattices. We believe that it is this diversity that gives new insights into the magnetic properties of (distorted) kagome antiferromagnets.

IV. CONCLUSIONS

We have studied crystal structure and magnetic properties of $\text{Cs}_2\text{LiTi}_3\text{F}_{12}$, which has an $S = 1/2$ distorted kagome lattice. The distortion of the kagome lattice is the largest among the four $A_2B\text{TiF}_{12}$ compounds. The temperature dependence of χ and the magnetization curve of $\text{Cs}_2\text{LiTi}_3\text{F}_{12}$ are very similar to those of $\text{Cs}_2\text{KTi}_3\text{F}_{12}$, which has the smallest distortion of the kagome lattice. However, density functional theory predicts different magnetic models for $\text{Cs}_2\text{LiTi}_3\text{F}_{12}$

and $\text{Cs}_2\text{KTi}_3\text{F}_{12}$. This is an indication that the electronic and magnetic anisotropy of the compounds cannot be read off in a simple way from the structural distortion. The magnetic model of $\text{Cs}_2\text{LiTi}_3\text{F}_{12}$ consists of antiferromagnetically coupled spin chains and anisotropic Δ chains. Both our experiment and numerical diagonalization study reveal that this system exhibits $1/3$ and 0.8 magnetization plateaus. It is an interesting open question if the new material $\text{Cs}_2\text{LiTi}_3\text{F}_{12}$ has a spin gap.

ACKNOWLEDGMENTS

This work was partly supported by JSPS KAKENHI Grants No. 18H01179, No. 16K05418, No. 16K05419, No. 16H01080 (JPhysics), and No. 18H04330 (JPhysics). Non-hybrid thread-parallel calculations in numerical diagonalizations were based on TITPACK version 2 coded by H. Nishimori. In this research, we used the computational resources of the K computer provided by the RIKEN Advanced Institute for Computational Science through the HPCI System Research project (Project ID: hp190053). We also used the computational resources of Fujitsu PRIMERGY CX600M1/CX1640M1(Oakforest-PACS) provided by Joint Center for Advanced High Performance Computing through the HPCI System Research projects (Project ID: hp180053 and hp190041). Some of the computations were performed using the facilities of the Department of Simulation Science, National Institute for Fusion Science; Institute for Solid State Physics, The University of Tokyo; and Supercomputing Division, Information Technology Center, The University of Tokyo.

-
- [1] C. Lacroix, P. Mendels, and F. Mila (eds.), *Introduction to Frustrated Magnetism* (Springer, Berlin, 2011).
- [2] L. Balents, Spin liquids in frustrated magnets, *Nature (London)* **464**, 199 (2010).
- [3] M. P. Shores, E. A. Nytko, B. M. Bartlett, and D. G. Nocera, A structurally perfect $S = 1/2$ kagomé antiferromagnet, *J. Am. Chem. Soc.* **127**, 13462 (2005).
- [4] H. Yoshida, Y. Michiue, E. Takayama-Muromachi, and M. Isobe, β -Vesignieite $\text{BaCu}_3\text{V}_2\text{O}_8(\text{OH})_2$: A structurally perfect $S = 1/2$ kagomé antiferromagnet, *J. Mater. Chem.* **22**, 18793 (2012).
- [5] M. Yoshida, Y. Okamoto, M. Takigawa, and Z. Hiroi, Magnetic order in the spin-1/2 kagome antiferromagnet vesignieite, *J. Phys. Soc. Jpn.* **82**, 013702 (2013).
- [6] R. H. Colman, A. Sinclair, and A. S. Wills, Comparisons between haydeeite, α - $\text{Cu}_3\text{Mg}(\text{OD})_6\text{Cl}_2$, and kapellasite, α - $\text{Cu}_3\text{Zn}(\text{OD})_6\text{Cl}_2$, isostructural $S = 1/2$ kagome magnets, *Chem. Mater.* **22**, 5774 (2010).
- [7] H. Yoshida, N. Noguchi, Y. Matsushita, Y. Ishii, Y. Ihara, M. Oda, H. Okabe, S. Yamashita, Y. Nakazawa, A. Takata, T. Kida, Y. Narumi, and M. Hagiwara, Unusual magnetic state with dual magnetic excitations in the single crystal of $S = 1/2$ kagome lattice antiferromagnet $\text{CaCu}_3(\text{OH})_6\text{Cl}_2 \cdot 0.6\text{H}_2\text{O}$, *J. Phys. Soc. Jpn.* **86**, 033704 (2017).
- [8] T. Ono, K. Morita, M. Yano, H. Tanaka, K. Fujii, H. Uekusa, Y. Narumi, and K. Kindo, Magnetic susceptibilities in a family of $S = 1/2$ kagome antiferromagnets, *Phys. Rev. B* **79**, 174407 (2009).
- [9] Ph. Mendels and F. Bert, Quantum kagome antiferromagnet $\text{ZnCu}_3(\text{OH})_6\text{Cl}_2$, *J. Phys. Soc. Jpn.* **79**, 011001 (2010).
- [10] M. Goto, H. Ueda, C. Michioka, A. Matsuo, K. Kindo, and K. Yoshimura, Various disordered ground states and $\frac{1}{3}$ magnetization-plateau-like behavior in the $S = \frac{1}{2}$ Ti^{3+} kagome lattice antiferromagnets $\text{Rb}_2\text{NaTi}_3\text{F}_{12}$, $\text{Cs}_2\text{NaTi}_3\text{F}_{12}$, and $\text{Cs}_2\text{KTi}_3\text{F}_{12}$, *Phys. Rev. B* **94**, 104432 (2016).
- [11] M. Goto, H. Ueda, C. Michioka, A. Matsuo, K. Kindo, K. Sugawara, S. Kobayashi, N. Katayama, H. Sawa, and K. Yoshimura, Ising-like anisotropy stabilized $1/3$ and $2/3$ magnetization plateaus in the V^{3+} kagome lattice antiferromagnets $\text{Cs}_2\text{KV}_3\text{F}_{12}$, $\text{Cs}_2\text{NaV}_3\text{F}_{12}$, and $\text{Rb}_2\text{NaV}_3\text{F}_{12}$, *Phys. Rev. B* **95**, 134436 (2017).
- [12] M. Goto, H. Ueda, C. Michioka, A. Matsuo, K. Kindo, K. Sugawara, S. Kobayashi, N. Katayama, H. Sawa, and K. Yoshimura, In-plane spin canting and $1/3$ -magnetization-plateau-like behavior in $S = 3/2$ Cr^{3+} kagome lattice antiferromagnets $\text{Cs}_2\text{KCr}_3\text{F}_{12}$ and $\text{Cs}_2\text{NaCr}_3\text{F}_{12}$, *Phys. Rev. B* **97**, 224421 (2018).
- [13] H. O. Jeschke, H. Nakano, and T. Sakai, From kagome strip to kagome lattice: Realizations of frustrated $S = 1/2$ antiferromagnets in Ti(III) fluorides, *Phys. Rev. B* **99**, 140410(R) (2019).

- [14] G. M. Sheldrick, computer code SHELXL-97, *Program for Structure Refinement* (University Göttingen, Germany, 1997).
- [15] K. Koepernik and H. Eschrig, Full-potential nonorthogonal local-orbital minimum-basis band-structure scheme, *Phys. Rev. B* **59**, 1743 (1999).
- [16] J. P. Perdew, K. Burke, and M. Ernzerhof, Generalized Gradient Approximation Made Simple, *Phys. Rev. Lett.* **77**, 3865 (1996).
- [17] A. I. Liechtenstein, V. I. Anisimov, and J. Zaanen, Density-functional theory and strong interactions: Orbital ordering in Mott-Hubbard insulators, *Phys. Rev. B* **52**, 5467(R) (1995).
- [18] T. Mizokawa and A. Fujimori, Electronic structure and orbital ordering in perovskite-type $3d$ transition-metal oxides studied by Hartree-Fock band-structure calculations, *Phys. Rev. B* **54**, 5368 (1996).
- [19] H. O. Jeschke, F. Salvat-Pujol, and R. Valentí, First-principles determination of Heisenberg Hamiltonian parameters for the spin-1/2 kagome antiferromagnet $\text{ZnCu}_3(\text{OH})_6\text{Cl}_2$, *Phys. Rev. B* **88**, 075106 (2013).
- [20] D. Guterding, R. Valentí, and H. O. Jeschke, Reduction of magnetic interlayer coupling in barlowite through isoelectronic substitution, *Phys. Rev. B* **94**, 125136 (2016).
- [21] Y. Iqbal, T. Müller, K. Riedl, J. Reuther, S. Rachel, R. Valentí, M. J. P. Gingras, R. Thomale, and H. O. Jeschke, Signatures of a gearwheel quantum spin liquid in a spin-1/2 pyrochlore molybdate Heisenberg antiferromagnet, *Phys. Rev. Mater.* **1**, 071201(R) (2017).
- [22] H. Nakano and A. Terai, Reexamination of finite-lattice extrapolation of Haldane gaps, *J. Phys. Soc. Jpn.* **78**, 014003 (2009).
- [23] H. Nakano and T. Sakai, Numerical-diagonalization study of spin gap issue of the kagome lattice Heisenberg antiferromagnet, *J. Phys. Soc. Jpn.* **80**, 053704 (2011).
- [24] H. Nakano, S. Todo, and T. Sakai, Long-range order of the three-sublattice structure in the $S = 1/2$ Heisenberg antiferromagnet on a spatially anisotropic triangular lattice, *J. Phys. Soc. Jpn.* **82**, 043715 (2013).
- [25] H. Nakano and T. Sakai, Anomalous behavior of the magnetization process of the $S = 1/2$ kagome-lattice Heisenberg antiferromagnet at one-third height of the saturation, *J. Phys. Soc. Jpn.* **83**, 104710 (2014).
- [26] H. Nakano and T. Sakai, Magnetization process of the spin- S kagome-lattice Heisenberg antiferromagnet, *J. Phys. Soc. Jpn.* **84**, 063705 (2015).
- [27] H. Nakano, Y. Hasegawa, and T. Sakai, Magnetization jump in the magnetization process of the spin-1/2 Heisenberg antiferromagnet on a distorted square-kagome lattice, *J. Phys. Soc. Jpn.* **84**, 114703 (2015).
- [28] H. Nakano and T. Sakai, Ferrimagnetism in the spin-1/2 Heisenberg antiferromagnet on a distorted triangular lattice, *J. Phys. Soc. Jpn.* **86**, 063702 (2017).
- [29] H. Nakano and T. Sakai, Magnetization process of the spin-1/2 triangular-lattice Heisenberg antiferromagnet with next-nearest-neighbor interactions—Plateau or nonplateau, *J. Phys. Soc. Jpn.* **86**, 114705 (2017).
- [30] H. Nakano and T. Sakai, Numerical-diagonalization study of magnetization process of frustrated spin-1/2 Heisenberg antiferromagnets in two dimensions: Triangular- and kagome-lattice antiferromagnets, *J. Phys. Soc. Jpn.* **87**, 063706 (2018).
- [31] Y. Hasegawa, H. Nakano, and T. Sakai, Metamagnetic jump in the spin-1/2 antiferromagnetic Heisenberg model on the square kagome lattice, *Phys. Rev. B* **98**, 014404 (2018).
- [32] T. Sakai and H. Nakano, Ground state with nonzero spontaneous magnetization of the two-dimensional spin-1/2 Heisenberg antiferromagnet with frustration, *AIP Adv.* **8**, 101408 (2018).
- [33] H. Nakano and T. Sakai, Precise estimation of the $S = 2$ Haldane gap by numerical diagonalization, *J. Phys. Soc. Jpn.* **87**, 105002 (2018).
- [34] H. Nakano and T. Sakai, Third boundary of the Shastry-Sutherland model by numerical diagonalization, *J. Phys. Soc. Jpn.* **87**, 123702 (2018).
- [35] H. Nakano, N. Todoroki, and T. Sakai, Haldane gaps of large- S Heisenberg antiferromagnetic chains and asymptotic behavior, *J. Phys. Soc. Jpn.* **88**, 114702 (2019).
- [36] D. Babel, Die struktur des RbNiCrF_6 -typs und ihre beziehung zur pyrochlorstruktur, *Z. Anorg. Allg. Chem.* **387**, 161 (1972).
- [37] L. J. de Jongh and A. R. Miedema, Experiments on simple magnetic model systems, *Adv. Phys.* **50**, 947 (2001).
- [38] N. Elstner and A. P. Young, Spin- $\frac{1}{2}$ Heisenberg antiferromagnet on the kagome lattice: High-temperature expansion and exact-diagonalization studies, *Phys. Rev. B* **50**, 6871 (1994).
- [39] K. Morita, M. Yano, T. Ono, H. Tanaka, K. Fujii, H. Uekusa, Y. Narumi, and K. Kindo, Singlet ground state and spin gap in $S = 1/2$ kagome antiferromagnet $\text{Rb}_2\text{Cu}_3\text{SnF}_{12}$, *J. Phys. Soc. Jpn.* **77**, 043707 (2008).
- [40] R. B. Griffiths, Magnetization curve at zero temperature for the antiferromagnetic Heisenberg linear chain, *Phys. Rev.* **133**, A768 (1964).
- [41] J. Richter, O. Derzhko and A. Honecker, The sawtooth chain: From Heisenberg spins to Hubbard electrons, *Int. J. Mod. Phys.* **22**, 4418 (2008).